

# Dual-Polarization FBMC for Improved Performance in Wireless Communication Systems

Hosseinali Jamal, *Member, IEEE*, David W. Matolak, *Senior Member, IEEE*

**Abstract**—Filter bank multi-carrier (FBMC) offers superior spectral properties compared to cyclic-prefix orthogonal frequency-division multiplexing (CP-OFDM), at the cost of an inherent shortcoming in dispersive channels called *intrinsic imaginary interference*. In this paper we propose a new FBMC based communication system using two orthogonal polarizations for wireless communication systems: dual-polarization FBMC (DP-FBMC). Using this system we can significantly suppress the FBMC intrinsic interference. Therefore in DP-FBMC all the multicarrier techniques used in CP-OFDM systems for channel equalization, multiple-input/multiple-output (MIMO) processing, etc., should be applicable without using the complex processing methods required for conventional FBMC. DP-FBMC also has other interesting advantages over CP-OFDM and FBMC: it is more robust in dispersive channels, and also to receiver carrier frequency offset (CFO) and timing offset (TO). In our DP-FBMC system we propose three different structures based on different multiplexing techniques. We show that compared to conventional FBMC, one of these DP-FBMC structures has equivalent complexity and equipment requirements. We compare DP-FBMC with other systems through simulations. According to our results DP-FBMC has potential as a promising candidate for future wireless communication networks.<sup>1</sup>

**Index Terms**—Dual Polarization-FBMC-MIMO-CP-OFDM-OQAM-FFT-CFO-TO

## I. INTRODUCTION

The orthogonal frequency division multiplexing (OFDM) modulation with the cyclic prefix (CP) extension is at present the most widespread multicarrier communication technique, due to its relative simplicity and robustness against multipath frequency selective channels thanks to the CP. Yet this inserted CP decreases the spectral efficiency, especially in highly-dispersive channels. Also, because of the symbol-time-limited pulses the OFDM spectrum is not compact, and has large spectral sidelobes, and it thus requires a large number of guard subcarriers to reduce the out-of-band power emission, further decreasing spectral efficiency. As an alternative approach to increase the spectral efficiency and offering a more compact power spectral density, filterbank multicarrier (FBMC) has been proposed [1]. The FBMC structure does not require a CP and has very compact spectral shape due to filtering. In many cases this can enhance the spectrum efficiency (throughput) significantly. FBMC has been studied and compared to CP-OFDM for future cellular communication networks such as 5G in [5], [7], and [10]. In the literature

several FBMC systems have been proposed and reviewed in recent years. These systems are based on different structures, many of which are listed in [2]-[5]. In this paper we focus on the most widespread and popular FBMC technique based on Saltzberg's method [6] (known as staggered multitone (SMT) FBMC [2] or OFDM-OQAM). This method makes it possible to have symbol-rate spacing between adjacent subcarriers without intersymbol interference (ISI) and intercarrier interference (ICI) in distortionless channels by introducing a shift of half the symbol period between the in-phase and quadrature components of QAM symbols. Thus in FBMC, the subcarrier symbols are modulated with real offset-QAM (OQAM) symbols and the orthogonality conditions are considered only in the real domain [2]. According to this real orthogonality condition, FBMC incurs a shortcoming due to "intrinsic imaginary interference" in dispersive channels. In the literature there are several proposals for estimating and mitigating intrinsic interference, but all these techniques increase complexity [8]-[9], [15]-[19], and [20]-[24].

Polarization-division multiplexing (PDM) is a physical layer communication technique for multiplexing signals on electromagnetic waves of two orthogonal polarization signal states on the same carrier frequency. This technique has been proposed for microwave links such as satellite television to double the throughput [11], [12]. It has also been proposed for fiber optic communication using two orthogonal left- and right-hand circularly polarized light beams in the same light guide fiber [13], [14]. In terrestrial and air-to-ground (AG) wireless communication environments, due to the non-stability of antenna position and often rich scattering in the wireless channels, using this method (to double throughput) will often not be practical, and would require highly complex receivers to remove the interference resulting from the often small cross-polarization discrimination (XPD). In this paper, using the PDM technique we propose dual-polarization FBMC (DP-FBMC) not to double the capacity but rather to solve the intrinsic imaginary interference shortcoming of FBMC systems in dispersive channels. By using two polarizations in FBMC we basically add another dimension to suppress the intrinsic interference. We show that transmitting symbols on two orthogonal polarizations reduces the interference by a large extent, and in order to further suppress the remaining residual interference we suggest choosing prototype filters with near Nyquist characteristics, such as square-root raised cosine (SRRC) filters.

Using different multiplexing techniques we propose three different DP-FBMC approaches: time-polarization division

<sup>1</sup> This paper has been submitted to the *IEEE Transactions on Vehicular Technology (TVT)* for possible publication as well as a U.S. patent application.

multiplexing (TPDM), frequency-polarization division multiplexing (FPDM), and time-frequency-polarization division multiplexing (TFPDM). The difference in these methods is the location of transmitted FBMC OQAM symbols in the time, frequency, and polarization domains. In TPDM we separate adjacent FBMC symbols on two orthogonal polarizations multiplexed in time. In FPDM we separate adjacent subcarriers on two orthogonal polarizations multiplexed in frequency, and in TFPDM we isolate symbols on two orthogonal polarizations multiplexed both in time and frequency. We will show that in the TPDM and TFPDM structures, we can reduce the dominant adjacent-symbol impacts both in time and frequency that can cause intrinsic interference. We also show that the proposed DP-FBMC has better bit error ratio (BER) performance in fading channels compared to both CP-OFDM and FBMC, due to the increased suppression of the intrinsic interference via dual polarizations.

The remainder of this paper is organized as follows: in Section II we describe the OFDM-OQAM based FBMC system model. In Section III we describe our proposed DP-FBMC communication systems. In Section IV we provide the simulation results and compare CP-OFDM, conventional FBMC and DP-FBMC systems' performance in three different communication channel scenarios: an air-to-ground (AG) channel based on NASA measurements, and the pedestrian and vehicular "channel A" from ITU recommendations. We also compare power spectral density (PSD), and evaluate the performance degradation in low XPD conditions. In Section V we provide conclusions and suggested future work.

## II. FBMC SYSTEM MODEL

In the OFDM-OQAM form of FBMC, real valued OQAM symbols  $a_{n,m}$  are filtered through prototype filter  $h(t)$  and then modulated across  $N$  subcarriers as described by the following continuous form equation,

$$x(t) = \sum_{n=0}^{N-1} \sum_{m \in \mathbb{Z}} a_{n,m} h\left(t - m \frac{T}{2}\right) e^{\frac{j\pi n t}{T}} e^{j\theta_{n,m}}. \quad (1)$$

Prototype filter  $h(t)$  is a finite impulse response filter with a length  $L=KN$ , with  $K$  defined as the overlapping factor. In this equation  $\theta_{n,m} = \frac{\pi}{2}(n+m)$  is a phase term between adjacent subcarriers and symbols to satisfy the orthogonality condition in the real domain at the receiver [2], [3]. According to (1) symbols are offset or overlapped by half a symbol duration,  $T/2$ . For implementation, to reduce the complexity, a polyphase network (PPN) of prototype filters and fast and inverse fast Fourier transforms (FFT, IFFT) are used, as shown in Figure 1. For more details regarding the PPN structure and FFT implementation refer to [2], [5], or [25]. In Figure 1(a), for the FBMC transmitter, note that after the  $\pi/2$  phase shifts, the IFFT input symbols are either purely real or purely imaginary values. After the IFFT block, subcarriers will be filtered through the PPN network, and for each block of  $N$  input subcarriers, what comes out of the parallel to serial (P/S) conversion is a signal vector with the same length as the prototype filter. These symbol vectors are then overlapped or

offset by  $T/2$  to achieve maximum spectral efficiency. In these structures the major processing complexities are due to the IFFT, FFT, and PPN blocks.

In Figure 2 we depict a useful diagram called time-frequency phase-space lattice to illustrate the transmitted symbols in time, frequency, and phase. This figure shows the time-frequency lattice of FBMC symbols for an example of 16 subcarriers. Note that all symbols adjacent in time or frequency have a  $\pi/2$  phase shift between them (adjacent circles and squares) to satisfy the real orthogonality condition [2], thus in perfect (distortionless) channel conditions there is no ISI or ICI at the receiver.

As mentioned, one main shortcoming of FBMC compared to OFDM emanates from this real orthogonality, which will be violated in non-perfect channel conditions. This problem yields what is called intrinsic imaginary interference, and this makes the use of the straightforward OFDM channel equalization and MIMO techniques impractical in FBMC. In order to reduce this interference for channel equalization and MIMO purposes, several methods have been proposed in recent years. Among these techniques are scattered or auxiliary pilots [15], [16], preamble-based channel estimation [17], spreading techniques for MIMO applications [18], and per-subchannel equalizers based on the frequency sampling approach for multi-antenna receivers [19].

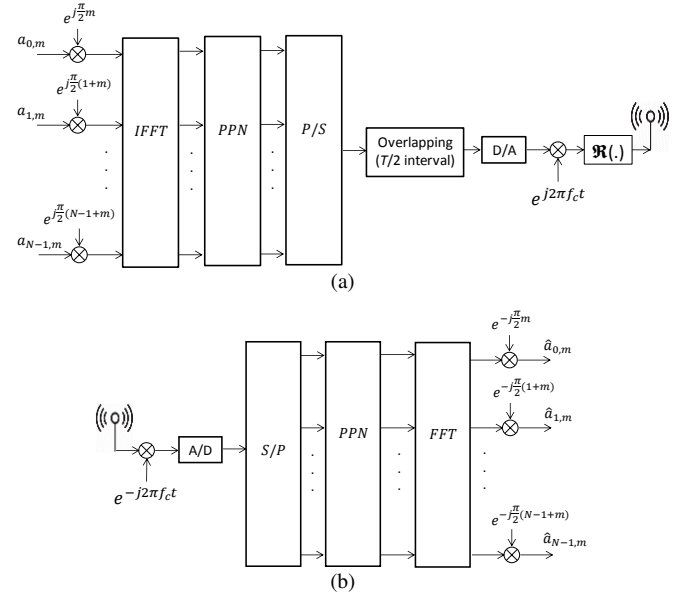


Figure 1. OQAM-OFDM (FBMC) communication system; (a) transmitter, (b) receiver.

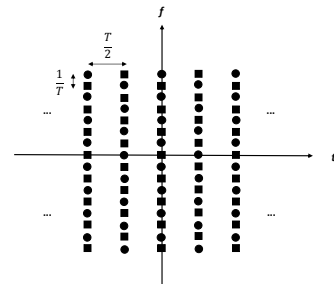


Figure 2. FBMC symbols time-frequency phase-space lattice ( $N=16$ ). Circles and squares denote a relative  $\pi/2$  phase shift between symbols adjacent in time and/or frequency.

All of these methods add extra computational complexity at receivers. In this paper we show that in DP-FBMC systems we can suppress the intrinsic imaginary interference very effectively without any extra processing.

We first analyze this intrinsic imaginary interference in conventional FBMC since this is useful to explain DP-FBMC as well. We rearrange (1) as follows,

$$x(t) = \sum_{n=0}^{N-1} \sum_{m=-\infty}^{\infty} a_{n,m} Q_{n,m}(t) \quad (2)$$

where,

$$Q_{n,m}(t) = h\left(t - m\frac{T}{2}\right) e^{j\frac{2\pi}{T}nt} e^{j\theta_{n,m}}. \quad (3)$$

Here the  $Q_{n,m}(t)$  functions are the time- and frequency-shifted versions of the prototype filter  $h(t)$ . Now assuming a perfect distortionless channel and with  $\theta_{n,m}$  as described in (1), the real orthogonality condition can be expressed as,

$$\Re\{\langle Q_{n,m}, Q_{p,q} \rangle\} = \Re\left\{ \int Q_{n,m}(t) Q_{p,q}^*(t) dt \right\} = \delta_{n,p} \delta_{m,q} \quad (4)$$

where  $\delta_{n,p}$  is the Kronecker delta, equal to 1 if  $n=p$  and 0 if  $n \neq p$ . After some calculations, and assuming perfect synchronization, one can express the received symbol estimates as follows,

$$\hat{a}_{n,m} = H_{n,m}(a_{n,m} + jI_{n,m}) + N_{n,m} \quad (5)$$

where  $H_{n,m}$  denotes the complex channel transfer function sample at subcarrier  $n$  and symbol  $m$ ,  $I_{n,m}$  is the intrinsic interference, and  $N_{n,m}$  is the additive white Gaussian noise (AWGN) variable at subcarrier  $n$  and symbol index  $m$ . As long as  $I_{n,m}$  is unknown at the receiver the application of pilot scattering channel estimation and therefore MIMO are extremely complex. Therefore for channel equalization and MIMO applications we must mitigate this interference. In [15] and later in [16] the authors proposed the use of auxiliary symbols adjacent to actual pilots: these auxiliary symbols are allocated to effectively remove  $I_{n,m}$  interference. These processing methods add slightly more complexity to the system. In this paper we will show that DP-FBMC structures (except one) substantially suppress  $I_{n,m}$  on all symbols without adding any more processing for channel equalization.

For calculating the  $I_{n,m}$  values we define the filter time-frequency localization samples as follows,

$$Q_{n,m}^{p,q} = -j\langle Q_{n,m}, Q_{p,q} \rangle = -j\left\{ \int Q_{n,m}(t) Q_{p,q}^*(t) dt \right\} \quad (6)$$

According to (4) - (6) we can easily state that the  $Q_{n,m}^{p,q}$  values are purely real. From the purely real or imaginary symbols surrounding the transmitted symbols we can calculate the intrinsic interference by the following summation,

$$I_{n,m} = \sum_{(p,q) \in \vartheta_{\Delta n, \Delta m}} a_{n+p, m+q} Q_{n,m}^{p,q} \quad (7)$$

where,

$$\vartheta_{\Delta n, \Delta m} = \{(p, q) : |p| \leq \Delta n, |q| \leq \Delta m \mid H_{n+p, m+q} \cong H_{n,m}\} \quad (8)$$

Now by defining a reference symbol  $a_{0,0}$ ,  $\vartheta_{\Delta n, \Delta m}$  is the set of

nearby indices within  $\Delta n$  subcarriers and  $\Delta m$  symbols of the reference subcarrier and symbol indices ( $n=0, m=0$ ). This assumption is true if the channel has an approximately equal response on nearby subcarriers, which is often valid for a variety of practical channels and appropriately selected inter-subcarrier frequency separations. In practice by choosing well-localized prototype filters,  $\Delta n, \Delta m$  can be as small as 1 [4], which means most of the intrinsic interference comes from the adjacent subcarriers and symbols, thus interference from symbols outside the neighborhood ( $\vartheta_{\Delta n, \Delta m}$ ) is negligible, i.e.,  $Q_{0,0}^{p,q}$  decreases as  $\Delta n$  and  $\Delta m$  increase.

### III. PROPOSED DP-FBMC SYSTEM MODEL

In Figure 3 we illustrate a dual polarization communication system using vertical and horizontal polarization antennas. In our DP-FBMC proposal we describe three different multiplexing approaches. In Figure 4 we depict the time-frequency-polarization phase-lattice of all DP-FBMC structures. In Figure 4(a) DP-FBMC *Structure I* based on TPDM is depicted. In this method we separate or isolate adjacent symbols on two orthogonal polarizations by multiplexing symbols in time. By this approach we can remove the intrinsic interference that results from (temporally) adjacent symbols. Interference still exists from symbols on nearby subcarriers.

In the DP-FBMC *Structure II* based on FPDM, as shown in Figure 4(b), we separate or isolate the adjacent transmitting subcarriers on two polarizations by multiplexing symbols in frequency. This method is not as useful as the first and third structures in removing intrinsic interference because most of the intrinsic interference comes from directly adjacent symbols on the same subcarrier index (at the same frequency, i.e., adjacent symbols on same row). Here we note that this method could also be used in OFDM. In Figure 4(c) we depict the time-frequency-polarization phase-lattice structure of DP-FBMC *Structure III* based on TFPDM. In this structure we transmit two halves of the OQAM symbols on two orthogonal polarizations at every symbol time, and then subsequently switch the order of half the subcarriers on the two polarizations at the next symbol time. Basically every other subcarrier is transmitted on a given polarization and the order is switched at each symbol interval. Hence if polarization isolation is perfect, the majority of the intrinsic imaginary interference (from nearest neighbor symbols) will be removed.

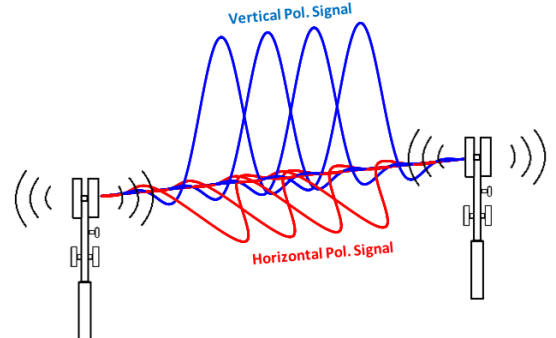


Figure 3. DP-FBMC wireless communication link (*Structure I*).

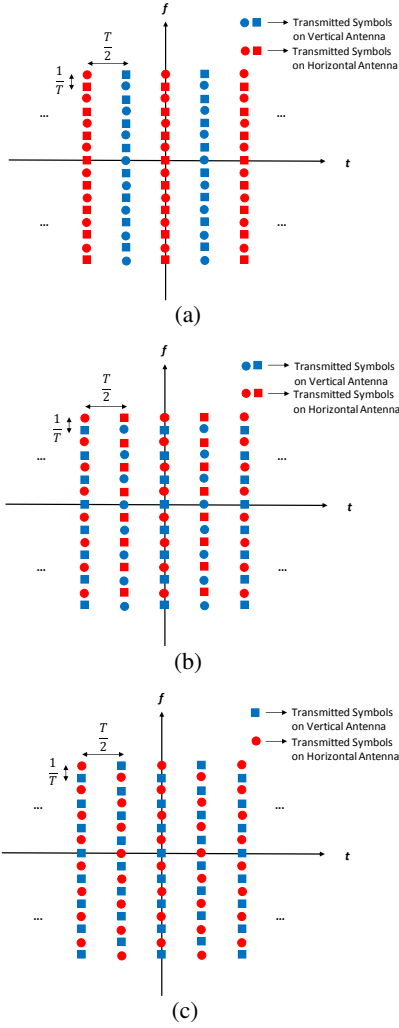


Figure 4. DP-FBMC symbols time-frequency-polarization phase-lattice, (a) *Structure I* based on TPDM, (b) *Structure II* based on FPDM, (c) *Structure III* based on TFPDM.

To provide a numerical example, in Table 1 we show the  $Q_{0,0}^{p,q}$  intrinsic interference values surrounding each reference symbol ( $a_{0,0}$ ) using a well-localized and widely studied prototype filter, the PHYDYAS filter with overlapping factor  $K=8$  [25]. In this table, assuming *Structure III* for DP-FBMC, the red colored  $Q_{0,0}^{p,q}$  values represent the time-frequency filter response on the same polarization as the reference symbol, and the green colored  $Q_{0,0}^{p,q}$  values are on the other polarization which produce no interference on the subject symbol (assuming perfect polarization isolation). Thus the interference caused by adjacent subcarriers is suppressed significantly by the PDM technique but there are still symbols (red) on the same polarization that can cause interference.

Table 1. PHYDYAS prototype filter  $Q_{0,0}^{p,q}$  intrinsic interference values for  $p = [-2, 2]$ ,  $q = [-3, 3]$ , and  $K=8$ .

$p \setminus q$	-3	-2	-1	0	1	2	3
-2	-0.0822j	0	0	0	0	0	-0.0822j
-1	0.0596j	0.1268j	0.1912j	0.2181j	0.1912j	0.1268j	0.0596j
0	-0.0822j	0	0.5769j	$Q_{0,0}^{0,0}=1$	-0.5769j	0	-0.0822j
1	0.0596j	-0.1268j	0.1912j	-0.2181j	0.1912j	-0.1268j	0.0596j
2	0	0	0	0	0	0	0

Table 2. SRRC prototype filter  $Q_{0,0}^{p,q}$  values for  $p = [-2, 2]$ ,  $q = [-3, 3]$ ,  $K=8$ , and  $\alpha=2/K=0.25$ .

$p \setminus q$	-3	-2	-1	0	1	2	3
-2	-0.1857j	0	0	0	0	0	-0.1857j
-1	0.0646j	0.0695j	0.0725j	0.0735j	0.0725j	0.0694j	0.0646j
0	0.1857j	0	0.6278j	$Q_{0,0}^{0,0}=1$	-0.6279j	0	-0.1857j
1	0.0646j	-0.0695j	0.0725j	-0.0735j	0.0725j	-0.0694j	0.0646j
2	0	0	0	0	0	0	0

Table 3. SRRC prototype filter  $Q_{0,0}^{p,q}$  values for  $p = [-2, 2]$ ,  $q = [-3, 3]$ ,  $K=16$ , and  $\alpha=2/K=0.125$ .

$p \setminus q$	-3	-2	-1	0	1	2	3
-2	-0.2055j	0	0	0	0	0	-0.2055j
-1	0.0356j	0.0362j	0.0366j	0.0367j	0.0366j	0.0362j	0.0356j
0	-0.2055j	0	0.6345j	$Q_{0,0}^{0,0}$	-0.6345j	0	-0.2055j
1	0.0356j	-0.0362j	0.0366j	-0.0367j	0.0366j	-0.0362j	0.0356j
2	0	0	0	0	0	0	0

To suppress this residual intrinsic interference we can employ a different prototype filter. We turned to the classic SRRC filter with overlapping factor  $K$ . Via some numerical trials, we determined heuristically that a roll-off factor  $\alpha=2/K$  performs well (additional filter choices represent another area of future work). In Tables 2 and 3 we list the  $Q_{0,0}^{p,q}$  intrinsic interference values surrounding our reference symbol for two example SRRC filter overlapping factors:  $K=8$ , 16. Here we note that the red  $Q_{0,0}^{p,q}$  values for  $K=16$  are approximately half those for the SRRC filter with  $K=8$ .

Therefore choosing the SRRC filter, especially with larger overlapping factors, significantly reduces the filter response samples representing co-polarized intrinsic interference (red color filter time-frequency locations). From these tables and as mentioned before we recognize that the majority of the intrinsic interference results from the temporally adjacent symbols (on the same subcarrier,  $p=0$  and  $q=-1$ , 1) and this is exactly the reason why the DP-FBMC *Structure II* is not effective in removing the intrinsic interference. Hence if *Structure II* is used, even with dual polarization we need intrinsic interference cancellation techniques for channel equalization such as those in conventional FBMC. Henceforth we only show results for *Structures I* and *III*. For illustration, in Figure 5 we plot the normalized energy prototype filter impulse response for PHYDYAS with  $K=8$  and SRRC with  $K=8$ , 16.

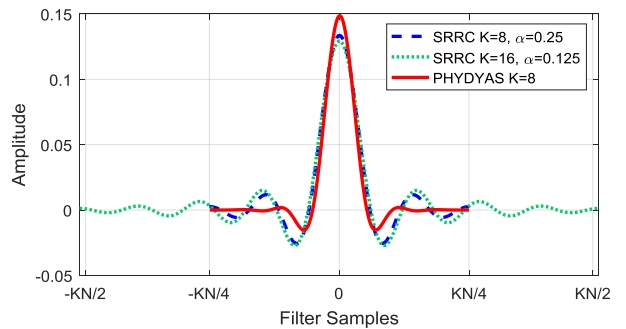


Figure 5. PHYDYAS and SRRC prototype filter impulse responses.

In (9), (10), and (11) we express the multiplexed OQAM symbols for DP-FBMC *Structures I*, *II*, and *III*, respectively,

$$a_{n,m}^H = \begin{cases} a_{n,m} & m \text{ even} \\ 0 & m \text{ odd} \end{cases}$$

$$a_{n,m}^V = \begin{cases} a_{n,m} & m \text{ odd} \\ 0 & m \text{ even} \end{cases}$$

$$a_{n,m}^H = \begin{cases} a_{n,m} & n \text{ even} \\ 0 & n \text{ odd} \end{cases}$$

$$a_{n,m}^V = \begin{cases} a_{n,m} & n \text{ odd} \\ 0 & n \text{ even} \end{cases}$$

$$a_{n,m}^H = \begin{cases} a_{n,m} & m \text{ even}, n \text{ even} \\ 0 & m \text{ even}, n \text{ odd} \\ 0 & m \text{ odd}, n \text{ even} \\ a_{n,m} & m \text{ odd}, n \text{ odd} \end{cases}$$

$$a_{n,m}^V = \begin{cases} a_{n,m} & m \text{ even}, n \text{ even} \\ a_{n,m} & m \text{ even}, n \text{ odd} \\ a_{n,m} & m \text{ odd}, n \text{ even} \\ 0 & m \text{ odd}, n \text{ odd} \end{cases}$$

Using (9)-(11) we express the transmitted waveforms on each polarization in (12). Note that we can also use circular right-handed and left-handed (or any other) orthogonal polarizations, but here we use the  $H$  and  $V$  notations for horizontal and vertical polarizations.

$$x^H(t) = \sum_{n=0}^{N-1} \sum_{m \in \mathbb{Z}} a_{n,m}^H h\left(t - m \frac{T}{2}\right) e^{\frac{j\pi n t}{T}} e^{j\theta_{n,m}}$$

$$x^V(t) = \sum_{n=0}^{N-1} \sum_{m \in \mathbb{Z}} a_{n,m}^V h\left(t - m \frac{T}{2}\right) e^{\frac{j\pi n t}{T}} e^{j\theta_{n,m}} \quad (12)$$

Figure 6 shows the DP-FBMC communication system block diagram for each polarization. Note that this figure applies to DP-FBMC *Structures II* and *III* but for *Structure I* we only need one IFFT and FFT at transmitter and receiver, and this is an advantage of *Structure I* compared to *Structures II* and *III* with respect to complexity.

We briefly compare the complexity of these structures with that of conventional FBMC. First considering the direct equation forms of (1) and (12), we find that in DP-FBMC *Structures II* and *III*, for each symbol period, the number of multiplications is reduced by a factor of two on each polarization as long as the input symbols on half the subcarriers are zero. Therefore the complexity of the DP-FBMC transmitter is similar to that of conventional FBMC. DP-FBMC *Structure I* also has complexity similar to that of conventional FBMC (based on the direct form).

If though we look at the fast implementation of the systems based on Figures 1 and 6, we deduce first that for DP-FBMC *Structures II* and *III* we need a second IFFT and FFT at both transmitter and receiver. Second we note that at every symbol time half of the subcarrier samples are zero so only half the subcarrier samples are needed at the receiver, therefore we can use the pruned IFFT/FFT algorithms [26]-[28] to reduce the added complexity. Based on Skinner's algorithms [27], pruning the vector of input samples with length  $N/2$  for an  $N$ -point IFFT requires  $2N \log_2(N/2)$  real multiplications and  $3N \log_2(N/2) + N$  real additions. Based on Markel's algorithm [26] pruning output samples with length  $N/2$  of an  $N$ -point FFT requires  $2N \log_2(N/4)$  real multiplications and  $3N \log_2(N/2)$  real additions [8].

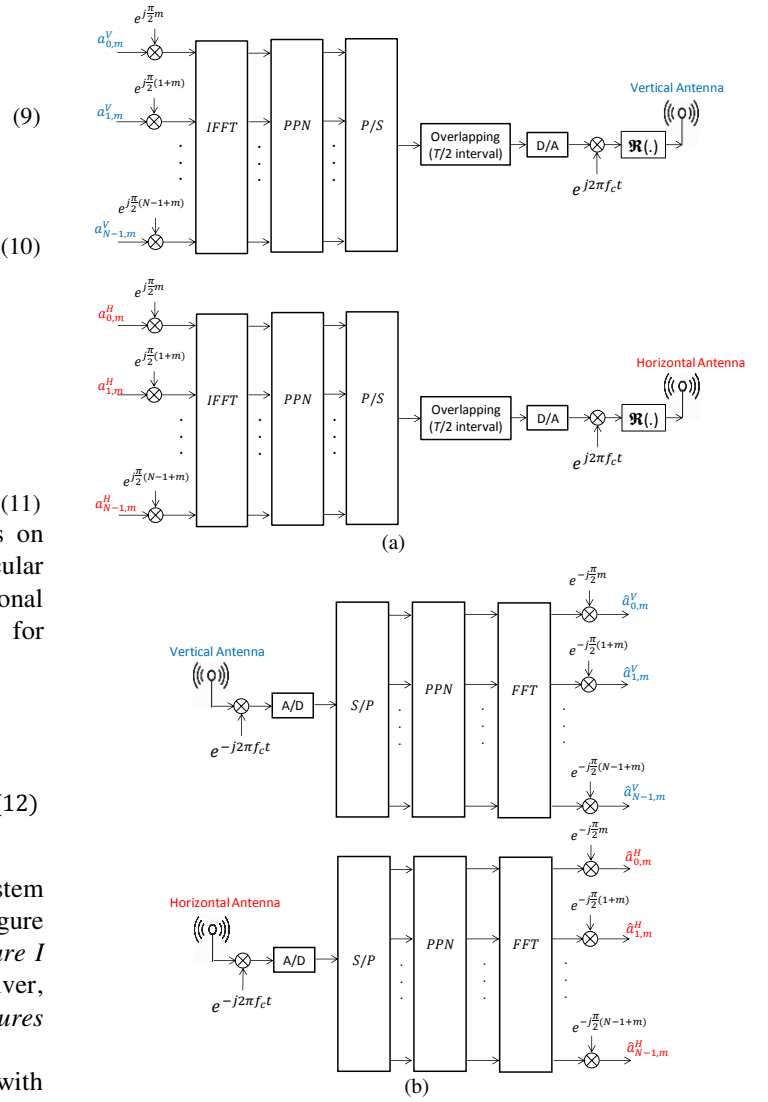


Figure 6. DP-FBMC communication system for *Structures II* and *III*; (a) transmitter, (b) receiver

The pruned IFFT/FFT is effective for a small number of subcarriers (e.g., less than 32), but for a large number of subcarriers this complexity reduction is not effective. After IFFT/FFT processing (*Structures II* and *III*) for PPN filtering we also need twice the multiplications of conventional FBMC. Therefore DP-FBMC *Structures II* and *III* have higher complexity than conventional FBMC. For *Structure I*, as long as we can share the same IFFT/FFT at every symbol period and polarization, we have the same complexity as conventional FBMC. A complete complexity analysis is also reserved for future work.

Regarding the transmit power in all structures, as long as half the symbols are nulled accordingly, each DP-FBMC antenna employs half the power of conventional FBMC, hence lower cost power amplifiers may be used. Received SNR or the energy per bit ( $E_b$ ) to noise density ratio  $E_b/N_0$  remains constant.

#### IV. SIMULATION RESULTS

In this section we compare the performance of CP-OFDM,

conventional FBMC, and DP-FBMC via computer simulations. At beginning simulation results we assume perfect XPD to illustrate the ideal DP-FBMC features; at the end we provide some results with realistic XPD values. We evaluate BER performance in different example channels, and the effects of carrier time and frequency offsets. We also compare the PSD of DP-FBMC using different prototype filters and overlapping factors. In addition, we evaluate the performance of DP-FBMC in the presence of polarization angular mismatch.

In Figure 7 we show the BER vs.  $E_b/N_0$  for CP-OFDM, FBMC and DP-FBMC communication systems for different modulation orders (QPSK, 16-QAM and 64-QAM), for three example channels. Here we note that *Structures I* or *III* yield identical BER results thus we only show the *Structure I* BER results. In these simulations there is no channel coding and we chose  $N=512$  subcarriers, 16 symbols per frame, and a channel bandwidth  $B=10$  MHz. Recall that on DP-FBMC *Structures I* and *III* adjacent symbols are separated on two orthogonal polarizations, therefore we expect the ISI caused from channel multipath delays will be lower than in conventional FBMC.

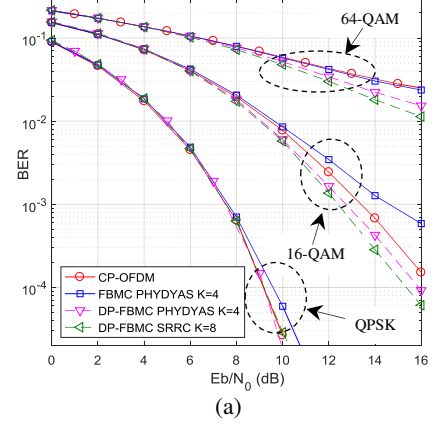
For the multipath channel fading models we used three different tapped delay line models for three different scenarios. The first channel model is an over-water strong line of sight (LOS) air-to-ground (AG) channel model based on NASA measurement results [29]. The second and third channels are the pedestrian and vehicular channel A from ITU-R Recommendation M.1225 [30]. In Table 4 we list the multipath power delay profiles for these channel models along with root-mean-square delay-spread (RMS-DS) values and fading models. In our analysis and BER performance simulation results, these channels represent mildly-dispersive, dispersive, and highly-dispersive channels. We use Ricean fading with Rice factor 30 dB for the strong LOS AG channel. For the pedestrian A channel, the first tap has Ricean fading with Rice factor 10 dB, with the remaining taps incurring Rayleigh fading. All taps in the vehicular A channel incur Rayleigh fading. In our simulations the transmitted signal is subject to slow fading for all cases. For example, at a 5 GHz carrier frequency and maximum velocity of 300 m/s for the AG case, the maximum Doppler shift is  $f_D = v/\lambda = 5$  kHz. Doppler spreads for the slower moving terrestrial platforms are orders of magnitude smaller. The channel coherence time, denoted  $T_c$ , is inversely proportional to Doppler spread, therefore for the AG case,  $T_c \cong 0.2$  ms. Thus as long as our 10 MHz bandwidth signal sample period is much smaller than  $T_c$ , the transmitted symbols are subjected to slow fading. In BER simulations we assume that any Doppler shifts are tracked and fully compensated at the receiver.

In the CP-OFDM transmitter, we ensure that the CP length is longer than the maximum delay spread of the multipath fading channel: this yields 1/16 of symbol period for the AG and pedestrian channel A, and 1/4 of symbol period for vehicular channel A. In all communication systems, we use 33 subcarriers as a typical number for guard band (17 on the left and 16 on the right of the signal spectrum), and also use a null DC subcarrier at the center of the spectrum.

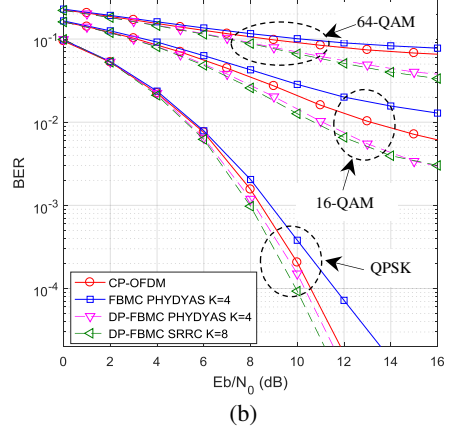
Table 4. Power delay profile, RMS-DS values, and fading models of example channel models.

Tap	AG LOS Channel		Pedestrian Channel A		Vehicular Channel A	
	$\tau$ (ns)	$\bar{P}$ (dB)	$\tau$ (ns)	$\bar{P}$ (dB)	$\tau$ (ns)	$\bar{P}$ (dB)
1	0	0	0	0	0	0
2	45	-12	110	-9.7	310	-1
3	200	-22.3	190	-19.2	710	-9
4			410	-22.8	1090	-10
5					1730	-15
6					2510	-20
RMS-DS (ns)	$\cong 18$		$\cong 46$		$\cong 370$	
Fading	Ricean (Rice factor 30 dB)		Ricean (Rice factor 10 dB)		Rayleigh	

Over-water AG Channel - QPSK, 16QAM, 64QAM- LS Equalization



Pedestrian Channel A- QPSK, 16QAM, 64QAM- LS Equalization



Vehicular Channel A- QPSK, 16QAM, 64QAM- LS Equalization

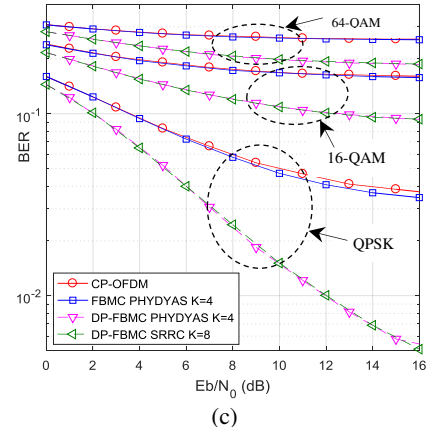


Figure 7. BER vs.  $E_b/N_0$  for QPSK, 16-QAM and 64-QAM modulations using LS channel equalization (a) over-water AG channel, (b) ITU pedestrian A channel, and (c) ITU vehicular B channel

For channel estimation we have 30 equally spaced subcarriers every 4 symbol periods as scattered pilots in all systems. For this pilot-based channel estimation, we used least square (LS) and discrete Fourier transform (DFT)-based interpolation techniques [33]. For the pilot-based channel estimation in conventional FBMC we used the auxiliary pilot technique based on [15], and assigned 1 auxiliary pilot symbol adjacent to each pilot symbol, and we chose  $p = [-2, 2]$ ,  $q = [-2, 3]$  for calculating the intrinsic interference  $Q_{n,m}^{p,q}$  values. Note that the total number of pilot symbols (including auxiliary symbols in FBMC) for channel equalization in all systems is the same, hence number of data symbols of all systems are identical. For DP-FBMC the auxiliary pilot symbol locations of conventional FBMC are allocated on the other polarization, therefore conventional FBMC and DP-FBMC have the same total number of allocated symbols for channel equalization. For the conventional FBMC simulations we chose the widely used PHYDYAS prototype filter for this system with  $K=4$  [24]. This prototype filter is of interest in conventional FBMC because of its good time-frequency localization. For DP-FBMC, as mentioned we used the SRRC filter with different overlapping factors  $K=4$  and  $8$  as well as PHYDYAS  $K=4$  for comparison. As a reminder in these simulations we use SRRC with roll-off factor  $\alpha=2/K$ .

According to the BER results DP-FBMC shows the best performance in all channel scenarios, especially in more dispersive channels. For example in vehicular A channel (Figure 7(c)) it outperforms CP-OFDM and conventional FBMC by approximately 5 dB at  $E_b/N_0=5 \times 10^{-2}$  with QPSK modulation. As noted, this better performance is because of lower ISI in DP-FBMC. Due to time multiplexing on both *Structures I* and *III*, the effective symbol separation on each polarization is larger than in conventional FBMC. This is why DP-FBMC has better performance, especially in highly frequency selective channels with long multipath delay spreads. Using the PHYDYAS filter in DP-FBMC yields slightly worse performance compared to that with the SRRC  $K=8$  filter, due to higher intrinsic interference. Here conventional FBMC has the worst performance because of intrinsic interference; this is most apparent in low dispersive channels such as AG and pedestrian A.

In Figure 8 we compare the PSD of these three systems obtained via the periodogram technique. First we note that we calculate these PSD results after removing the two ends of FBMC and DP-FBMC waveforms (resulting from filter tails) in order to reduce the frame lengths.

We truncated the first  $(K/2 - 1)N$  and last  $(K/2 - 1)N$  samples of each frame on both conventional FBMC and DP-FBMC waveforms. Note that for all FBMC systems this is the maximum acceptable truncation and further truncation will yield BER degradation. In Figure 10(a) we also show the PSD of CP-OFDM with and without windowing. In CP-OFDM windowing is used to reduce the out of band power. For our windowed CP-OFDM we used a raised cosine (RC) window. As expected, lengthening the filter (increasing  $K$ ) using SRRC yields smaller FBMC out of band power.

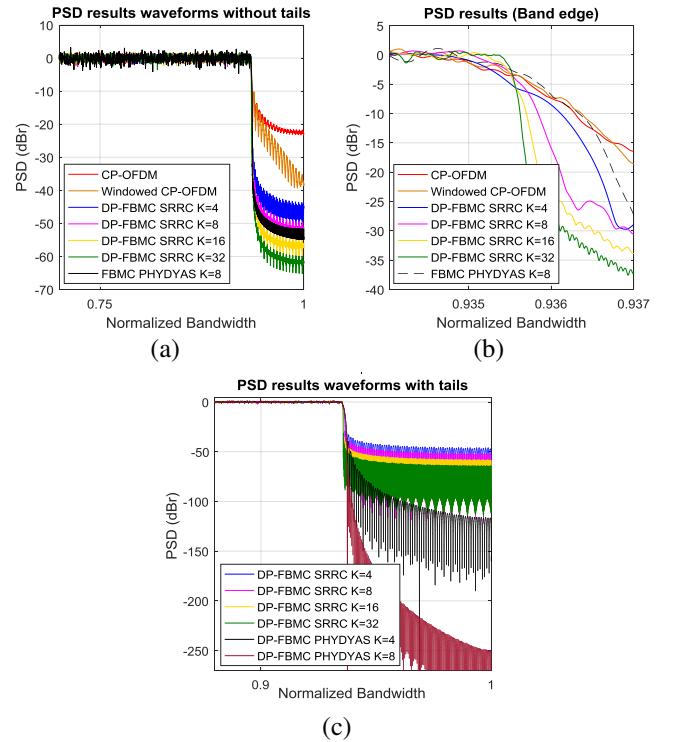


Figure 8. PSD vs. normalized bandwidth; (a) waveforms without tails, (b) around the band edge view, (c) waveforms including tails

In Figure 8(c) we also show the PSDs without truncation for comparison, and as expected the PHYDYAS filter has the best result. In Figure 8(b) we plotted the spectra of Figure 8(a) around the band edge. As expected, using SRRC filters with larger overlapping factors yields more compact power spectral densities. Thus after truncation DP-FBMC has a more compact PSD than conventional FBMC for the same  $K$ .

In Figure 9 we show BER versus carrier frequency and timing offsets at the receiver. We compared the results with some results in the literature [31], [32] and found our results consistent for FBMC and CP-OFDM. Note that here the BER is simulated in an AWGN channel with 16-QAM modulation and  $E_b/N_0 = 12$  dB with 512 subcarriers and the frame structure has 16 symbols per frame. The CFO values are normalized to the subcarrier bandwidth and timing offsets are in terms of the sampling period. We chose a channel bandwidth  $B=5$  MHz. These results illustrate the better performance of DP-FBMC in different frequency and timing offsets. We also note that longer overlapping factors in DP-FBMC yield better BER performance versus CFO and TO.

In all previous results we assumed perfect XPD (infinite) between the two received antenna's signals, which is not often a realistic assumption. In order to estimate the effect of imperfect XPD on DP-FBMC performance we consider two scenarios. In the first scenario we assume no XP interference due to imperfect antennas or rich scattering channel environments, but instead only assume an angular mismatch between the two (*linear*) polarizations. Therefore at each  $\theta$  degree angular mismatch the received electromagnetic wave amplitudes are scaled by factors of  $\cos(\theta)$  and  $\sin(\theta)$  multiplying the desired (co-) and undesired (cross-) polarization components, respectively.

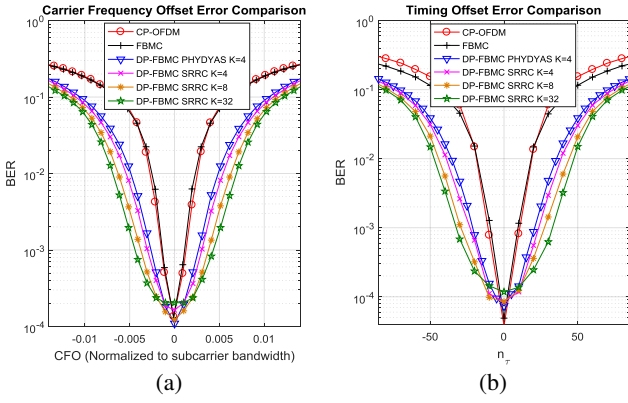


Figure 9. AWGN channel,  $E_b/N_0=12$  dB, 16-QAM, 512 subcarriers, and  $B=5$  MHz: (a) BER vs. CFO, (b) BER vs. TO

Figure 10 shows the BER vs.  $E_b/N_0$  results for different modulation orders in an AWGN channel (identical results for DP-FBMC Structures I and III). Using low modulation orders such as QPSK, DP-FBMC has acceptable performance even at polarization angular mismatches up to  $45^\circ$  (with a few dB loss in SNR), and this happens thanks to the  $\pi/2$  phase shifts ( $\theta_{n,m}$ ) between symbols according to (13). Based on these results the tolerance of the DP-FBMC system decreases for higher order modulations. The theoretical results for QPSK modulation are also shown in Figure 10-a. In this case the signal to interference plus noise ratio (SINR) equals  $\text{SNR} - 10\log(1 + \tan^2(\theta))$  dB where the subtracted term is the cross-polarization interference caused by the  $\theta^\circ$  angular mismatch. For other modulation types cross-polarization interference calculation is not as straightforward as PSK. In order to mitigate the interference from polarization mismatch we can use polarization interference cancellation (XPIC) techniques at the receivers. Naturally this improves performance at the expense of complexity. As future work for DP-FBMC we will explore this using pilot-sequence-based XPD estimation.

In a second scenario we simulate the BER performance for several practical XPD values using actual pilot-based LS channel estimation for 16-QAM and 64-QAM modulations. Here we assume orthogonal circular polarization or in the case of linear polarization we assume no XP due to angular mismatch.

We can express the XPD in the following equation forms for two cross-polarization cases on each antenna,

$$XPD_{VV} = 20 \log \left( \frac{h_{VV}}{h_{HV}} \right), \quad XPD_{HH} = 20 \log \left( \frac{h_{HH}}{h_{VH}} \right) \quad (13)$$

where  $h_{VV}$ ,  $h_{HH}$  are the narrowband co-polarization channel responses between (co-) polarized antennas and  $h_{HV}$ ,  $h_{VH}$  are the cross-polarized channel responses.

In Figure 11 simulation results for BER vs. XPD are shown assuming  $h_{HH} = h_{VV}$  and  $h_{HV} = h_{VH}$ . Here the multipath channel models we used are the pedestrian and vehicular channel A with bandwidth 10 MHz, and  $N=512$  subcarriers. For both 16-QAM, and 64-QAM modulations we chose  $E_b/N_0 = 16$  dB. Other physical layer parameters are identical to those used in Figure 7. Here for the SRRC prototype filter we chose

$K=8$ . As anticipated, smaller cross polarization discrimination degrades the performance, although XPD values from approximately 10-14 dB yield nearly ideal performance. In order to enhance the performance of DP-FBMC in weak XPD conditions we should investigate a method to estimate and remove the cross-polarization interference from received signals.

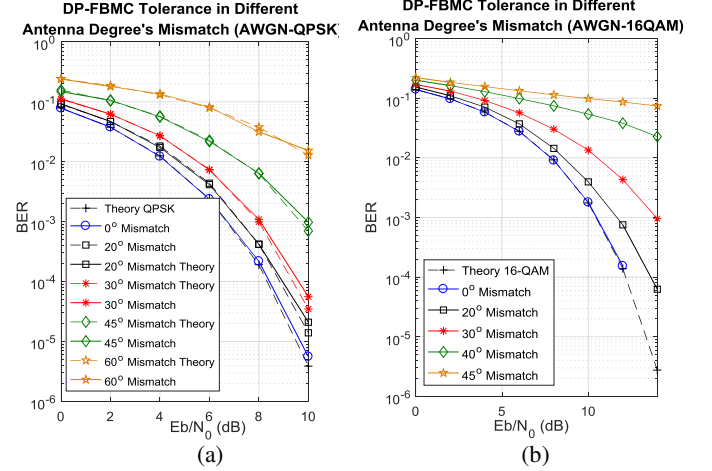


Figure 10. BER vs.  $E_b/N_0$  in different angular mismatch, AWGN channel; (a) QPSK, (b) 16-QAM modulation

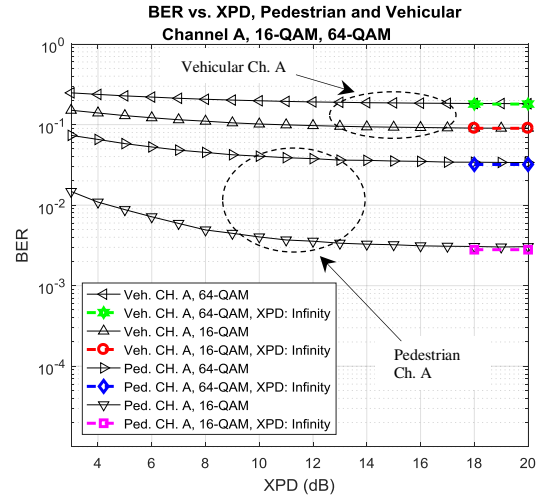


Figure 11. BER vs. XPD for 16-QAM and 64-QAM modulation orders in ITU pedestrian and vehicular channel A.  $E_b/N_0=16$  dB.

## V. CONCLUSION

In this paper we proposed a new FBMC system based on a dual polarization multiplexing technique. We showed that using specific time, frequency, and polarization multiplexing structures we can significantly suppress the intrinsic imaginary interference in FBMC systems. In good XPD conditions DP-FBMC provides better reliability and performance than conventional FBMC and CD-OFDM, particularly for more dispersive channels. DP-FBMC suffers in very small XPD conditions, therefore in future work we will investigate data based XPD estimation and cancellation techniques.

## REFERENCES

- [1] B. Le Floch, M. Alard and C. Berrou, "Coded orthogonal frequency division multiplex [TV broadcasting]," *Proceedings of the IEEE*, vol. 83, no. 6, pp. 982-996, Jun 1995.
- [2] P. Siohan, C. Siclet and N. Lacaille, "Analysis and design of OFDM/OQAM systems based on filterbank theory," *IEEE Transactions on Signal Processing*, vol. 50, no. 5, pp. 1170-1183, May 2002.
- [3] B. Farhang-Boroujeny, "OFDM Versus Filter Bank Multicarrier," *IEEE Signal Processing Magazine*, vol. 28, no. 3, pp. 92-112, May 2011.
- [4] B. Farhang-Boroujeny and C. H. Yuen, "Cosine modulated and offset QAM filter bank multicarrier techniques: a continuous-time prospect," *EURASIP J. Advances in Signal Process.*, vol. 2010, Jan. 2010.
- [5] B. Farhang-Boroujeny, "Filter Bank Multicarrier Modulation: A Waveform Candidate for 5G and Beyond," *Hindawi, Advances in Electrical Engineering*, vol. 2014, Article ID 482805, 25 pages, 2014.
- [6] B. Saltzberg, "Performance of an Efficient Parallel Data Transmission System," *IEEE Transactions on Communication Technology*, vol. 15, no. 6, pp. 805-811, December 1967.
- [7] F. Schaich and T. Wild, "Waveform contenders for 5G — OFDM vs. FBMC vs. U-FMC," *6th International Symposium on Communications, Control and Signal Processing (ISCCSP)*, Athens, 2014, pp. 457-460.
- [8] R. Zakaria and D. Le Ruyet, "A Novel Filter-Bank Multicarrier Scheme to Mitigate the Intrinsic Interference: Application to MIMO Systems," *IEEE Transactions on Wireless Communications*, vol. 11, no. 3, pp. 1112-1123, March 2012.
- [9] C. Kim, Y. H. Yun, K. Kim and J. Y. Seol, "Introduction to QAM-FBMC: From Waveform Optimization to System Design," *IEEE Communications Magazine*, vol. 54, no. 11, pp. 66-73, November 2016.
- [10] X. Zhang, L. Chen, J. Qiu and J. Abdoli, "On the Waveform for 5G," in *IEEE Communications Magazine*, vol. 54, no. 11, pp. 74-80, November 2016.
- [11] International Telecommunications Union (ITU), Report *ITU-R M.2175*, "Simultaneous dual linear polarization transmission technique using digital cross-polarization cancellation for MSS systems," July 2010.
- [12] P. D. Arapoglou, P. Burzigotti, M. Bertinelli, A. Bolea Alamanac and R. De Gaudenzi, "To MIMO or Not To MIMO in Mobile Satellite Broadcasting Systems," *IEEE Transactions on Wireless Communications*, vol. 10, no. 9, pp. 2807-2811, September 2011.
- [13] F. Horlin, J. Fickers, P. Emplit, A. Bourdoux, and J. Louveaux, "Dual-polarization OFDM-OQAM for communications over optical fibers with coherent detection," *Optics Express* 21, 6409-6421 (2013).
- [14] E. Giacomidis, M. Jarajreh, S. Sygletos, S. Le, F. Farjady, A. Tsokanos, A. Hamié, E. Pincemin, Y. Jaouën, A. Ellis, and N. Doran, "Dual-polarization multi-band optical OFDM transmission and transceiver limitations for up to 500 Gb/s uncompensated long-haul links," *Optics Express* 22, pp. 10975-10986 (2014).
- [15] J. P. Javaudin, D. Lacroix and A. Rouxel, "Pilot-aided channel estimation for OFDM/OQAM," *57th IEEE Vehicular Technology Conference*, VTC Spring, pp. 1581-1585, vol. 3, 2003.
- [16] C. Lele, R. Legouable and P. Siohan, "Channel estimation with scattered pilots in OFDM/OQAM," *IEEE 9th Workshop on Signal Processing Advances in Wireless Communications*, Recife, pp. 286-290, 2008.
- [17] C. Lele, P. Siohan, R. Legouable and J. P. Javaudin, "Preamble-based channel estimation techniques for OFDM/OQAM over the powerline," *IEEE International Symposium on Power Line Communications and its Applications*, Pisa, 2007, pp. 59-64, 2007.
- [18] R. Nissel and M. Rupp, "Enabling Low-Complexity MIMO in FBMC-OQAM," *IEEE Globecom Workshops (GC Wkshps)*, Washington, DC, pp. 1-6, 2016.
- [19] T. Ihalainen, A. Ikhlef, J. Louveaux and M. Renfors, "Channel Equalization for Multi-Antenna FBMC/OQAM Receivers," *IEEE Transactions on Vehicular Technology*, vol. 60, no. 5, pp. 2070-2085, Jun 2011.
- [20] U. Jayasinghe, N. Rajatheva and M. Latva-aho, "Application of a leakage based precoding scheme to mitigate intrinsic interference in FBMC," *IEEE International Conference on Communications (ICC)*, Budapest, 2013, pp. 5268-5272.
- [21] Y. Cheng, P. Li and M. Haardt, "Coordinated beamforming for the multi-user MIMO downlink using FBMC/OQAM," *6th International Symposium on Communications, Control and Signal Processing (ISCCSP)*, Athens, 2014, pp. 465-469.
- [22] J. Wang, Y. Zhang, H. Zhao, L. Li, H. Long and H. Shen, "A Novel QAM-FBMC without Intrinsic Time-Domain Interference," *IEEE 84th Vehicular Technology Conference (VTC-Fall)*, Montreal, QC, 2016, pp. 1-6.
- [23] J. Wang, H. Zhao, Y. Zhang, F. Li and L. Zhao, "Intrinsic Interference Elimination for Preamble-Based Channel Estimation in FBMC Systems," *IEEE Globecom Workshops (GC Wkshps)*, Washington, DC, 2016, pp. 1-5.
- [24] L. Häring, "Intrinsic interference-aware adaptive FBMC transmission with automatic modulation classification," *17th International Symposium on Communications and Information Technologies (ISCIT)*, Cairns, QLD, 2017, pp. 1-6.
- [25] M. Bellanger, et al. "FBMC physical layer: a primer." PHYDYAS, no. 4, Jan 2010. [Online]. Available: [http://www.ict-phydyas.org/teamspace/internal-folder/FBMC-Primer\\_06-2010.pdf](http://www.ict-phydyas.org/teamspace/internal-folder/FBMC-Primer_06-2010.pdf)
- [26] J. Markel, "FFT pruning," *IEEE Transactions on Audio and Electroacoustics*, vol. 19, no. 4, pp. 305-311, Dec 1971.
- [27] D. Skinner, "Pruning the decimation in-time FFT algorithm," *IEEE Transactions on Acoustics, Speech, and Signal Processing*, vol. 24, no. 2, pp. 193-194, Apr 1976.
- [28] H. V. Sorensen and C. S. Burrus, "Efficient computation of the DFT with only a subset of input or output points," in *IEEE Transactions on Signal Processing*, vol. 41, no. 3, pp. 1184-1200, Mar 1993.
- [29] D. W. Matolak and R. Sun, "Air-Ground Channel Characterization for Unmanned Aircraft Systems—Part I: Methods, Measurements, and Models for Over-Water Settings," *IEEE Transactions on Vehicular Technology*, vol. 66, no. 1, pp. 26-44, Jan. 2017.
- [30] International Telecommunications Union (ITU), Report *ITU-R M.1225*, "Guidelines for evaluation of radio transmission technologies for IMT-2000," Feb 1997.
- [31] D. Mattera, M. Tanda, M. Bellanger, "Frequency domain CFO compensation for FBMC systems," *Signal Processing, ScienceDirect*, Volume 114, Pages 183-197, ISSN 0165-1684, 2015.
- [32] D. Mattera, M. Tanda, M. Bellanger, "Performance analysis of some timing offset equalizers for FBMC/OQAM systems," *Signal Processing, ScienceDirect*, Volume 108, Pages 167-182, ISSN 0165-1684, 2015.
- [33] Y. S. Cho, J. Kim, W. Y. Yang, and C. G. Kang, *MIMO-OFDM Wireless Communications with MATLAB*. Singapore: John Wiley & Sons (Asia) Pte Ltd, 2010.